

# Journal of Materials Chemistry A

Accepted Manuscript



This is an *Accepted Manuscript*, which has been through the Royal Society of Chemistry peer review process and has been accepted for publication.

*Accepted Manuscripts* are published online shortly after acceptance, before technical editing, formatting and proof reading. Using this free service, authors can make their results available to the community, in citable form, before we publish the edited article. We will replace this *Accepted Manuscript* with the edited and formatted *Advance Article* as soon as it is available.

You can find more information about *Accepted Manuscripts* in the [Information for Authors](#).

Please note that technical editing may introduce minor changes to the text and/or graphics, which may alter content. The journal's standard [Terms & Conditions](#) and the [Ethical guidelines](#) still apply. In no event shall the Royal Society of Chemistry be held responsible for any errors or omissions in this *Accepted Manuscript* or any consequences arising from the use of any information it contains.

# Palladium nanoparticles *in situ* generated in metal-organic films for catalytic applications

*Shuiying Gao, Minna Cao, Weijin Li and Rong Cao\**

State Key Laboratory of Structural Chemistry, Fujian Institute of Research on the Structure of Matter, the Chinese Academy of Sciences, Fuzhou 350002, China

---

● To whom correspondence should be addressed.

## ABSTRACT

Palladium nanoparticles were firstly *in situ* generated in metal-organic films for catalytic applications. Layer-by-layer assembly of metal-organic films consisting of rigid-rod chromophores connected by terminal pyridine moieties to palladium centers on solid substrates was presented. Bipyridyl and polypyridyl ligands were used as building blocks in order to explore the influence of different ligand structures on the catalytic properties. Metal-organic films were characterized by UV-Vis spectra, atomic force images (AFM), transmission electron microscopy (TEM) and X-ray photoelectron spectroscopy (XPS). The results show that the deposition mechanism of metal-organic films is perfect layer-by-layer self-assembling with complete surface coverage and a regular growth. Moreover, the catalytic activity toward hydrogenation of olefin was investigated. Based on XPS and TEM, the catalytic activity toward hydrogenation of olefin was ascribed to the *in situ* formation of Pd nanoparticles from Pd ions in metal-organic films. This film material is a active catalyst for the hydrogenation of olefin under mild conditions. Furthermore, the catalytic results indicated that the monodentate bipyridyl ligands gave superior catalytic activity than tridentate polypyridyl ligands. The catalytic activity is related to the loading amount of catalysts and the permeability. More importantly, this study points toward the potential application of metal-organic films as heterogeneous catalysts with easy separation and good recyclability.

KEYWORDS: Pd nanoparticles, Layer-by-layer self-assembly, Metal-organic films, Olefin hydrogenation, Catalytic activity

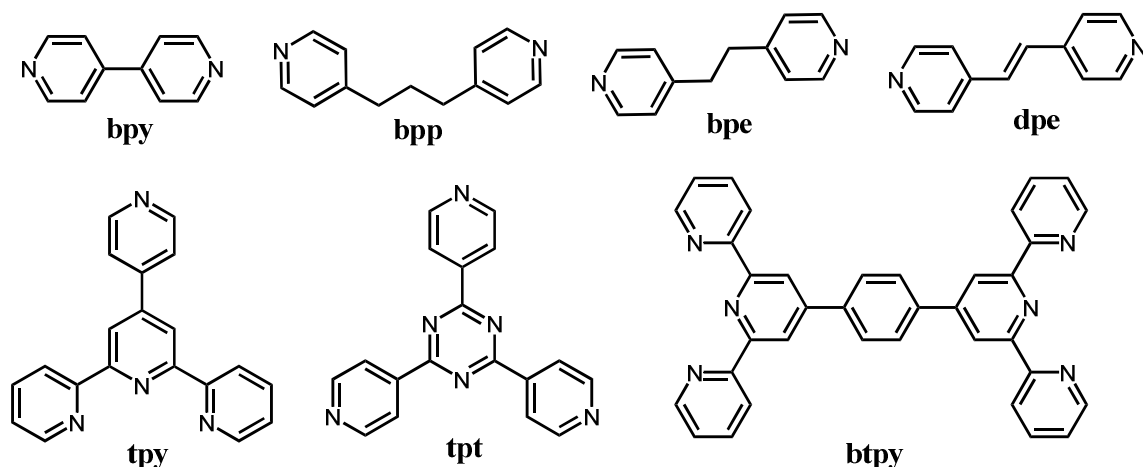
## 1 Introduction

Noble metal Pd nanoparticles (NPs) is widely used in hydrogenation reaction in petroleum refining industry. Due to the low storage capacity of the noble metals, decreasing the loading of noble metals is particularly important. Therefore, Pd NPs are usually loaded on solid substrates such as carbon and  $\text{Al}_2\text{O}_3$  as heterogeneous catalysts for recycling.<sup>1-7</sup> During the past few years, the application of catalytic films has attracted significant interest in heterogeneous catalytic technology.<sup>8</sup> The metal-organic films represent a new variety of catalysts due to their electronic, photonic and catalytic properties of metal ions.<sup>9, 10</sup> However, their applications in electro/or photo and catalytic devices were limited by their crystalline form. Layer-by-layer (LbL) assembly of metal-organic films can be simply achieved by alternating adsorption of metal precursor and ligand molecules through covalent or noncovalent interactions.<sup>11</sup> Noncovalent interactions, such as electrostatic interactions and direct metal ion-ligand interactions were most commonly involved in self-assembly LbL multilayers. For example, functional metal-organic complexes were loaded within LbL multilayers by alternate adsorption of palladium ion and pyridyl ligand layers onto solid slides through metal ion-ligand interactions.<sup>12-14</sup> Based on metal ion-ligand interactions between ruthenium ions and terpyridine ligands, metal-organic films consisting of ruthenium ions were prepared and exhibited the optoelectronic properties.<sup>15, 16</sup> Moreover, other metal ions such as zinc ions and cobalt ions were also assembled into films through the coordinative interactions between the tpy-groups and metal ions leading to electrochromic properties.<sup>17</sup> However, metal-organic films toward catalytic application have been rarely reported.

There are many reports on metallic Pd films using polyelectrolytes as building blocks, which have been explored as matrices for synthesis of zero-charge Pd NPs by  $\text{NaBH}_4$  reduction in order

to generate large surface area heterogeneous catalyst.<sup>18-22</sup> For example, Bruening and coauthors reported selective hydrogenation of unsaturated alcohols using LbL PAA/PEI-Pd(0) films on alumina particles (PAA =poly(acrylic acid, PEI =polyethylenimine).<sup>18-20</sup> Polymer matrices have also been utilized as solid supports because of the nature of macromolecular, which can control the size of nanoparticles and prevent the agglomeration of particles.<sup>2</sup> Polyethylene glycol (PEG) stabilized Pd NPs synthesized by Harraz and coauthors exhibited a remarkable catalytic activity toward hydrogenation reactions.<sup>1</sup> However, *in-situ* synthesis of Pd NPs within the LbL metal-organic films were rarely reported. The *in situ* self-assembly LbL multilayer nanoreactors possess several distinct advantages, such as tunable structure, variable composition and good chemical stability.

Based on metal ion-ligand interaction, small organic functional ligands (Scheme 1) can be used as building blocks to construct self-assembly LbL films. Each metal ion is separated and connected by organic ligands. We report here a self-assembly multilayer of metal-organic (Pd/Ligand)<sub>n</sub> films consisting of pyridyl ligand building blocks with characteristics of catalytic activity toward hydrogenation of olefin. The pyridyl ligands of different coordination mode such as monodentate and tridentate ligands were chosen in order to investigate the influence of ligand structures on the catalytic properties. X-ray photoelectron spectroscopy (XPS) and transmission electron microscope (TEM) investigation revealed that the noble metal ions (Pd<sup>2+</sup>) in metal-organic films are *in situ* reduced into Pd NPs during the hydrogenation of olefin process. The catalytic films are not desorbed from slides and showed good recyclability.



**Scheme 1** The chemical structures of the pyridyl ligands

## 2 Experimental materials and methods

### 2.1 Materials

Poly(ethylenimine) (PEI, MW = 6,000, 50 wt% aqueous solution), 4',4''-(1,4-Phenylene)bis(2,2':6',2''-terpyridine) (bitpy), trans-4-phenyl-3-buten-2-one, nitrobenzene and ethyl cinnamate were purchased from Aldrich Chemical Co. The ligand 1, 2-di(4-pyridyl)ethane (bpe) and 2, 4, 6-tri(4-pyridyl)-1,3,5-triazine (tpt) were purchased from TCI Chemical Co. The ligand 1, 3-di(4-pyridyl)propane were from Alfa Company. 4, 4'-bipyridyl (bpy), 1, 2-di(4-pyridyl)ethylene (dpe), styrene, linalool, 4-nitrostyrene and 4-bromostyrene were from J&K Chemical Company. (4'--(4-pyridyl)2,2':6',2''-terpyridine) (tpy) was synthesized according to the reference.<sup>23</sup> Millipore filtered water was used in all experiments (Milli-Q, 18.2 MΩ cm).

### 2.2 Preparation of (Pd/Ligand)<sub>n</sub> metal-organic films

The quartz slides (size 25 mm × 12 mm × 1 mm) (or single-crystal silicon slides) were cleaned with a “piranha solution” at 80 °C for 40 min, and thoroughly rinsed with water. Further purification was carried out by immersion in an H<sub>2</sub>O/H<sub>2</sub>O<sub>2</sub>/NH<sub>3</sub>OH (5:1:1) (V/V/V) bath for 30 min at 70 °C. The clean slides were first immersed in PEI solution for 20 min. (Pd/bpy)<sub>n</sub>, (Pd/bpe)<sub>n</sub>, (Pd/dpe)<sub>n</sub> and (Pd/bpp)<sub>n</sub> multilayers were prepared by alternately immersing quartz slide pre-coated with PEI layer in K<sub>2</sub>PdCl<sub>4</sub> aqueous solution (5 mM, 10 mL) and ligand (5 mM, 10 mL) ethanol solution. (Pd/tpt)<sub>n</sub>, (Pd/tpy)<sub>n</sub> and (Pd/bitpy)<sub>n</sub> multilayers were prepared by alternately immersing quartz slide pre-coated with PEI layer in K<sub>2</sub>PdCl<sub>4</sub> aqueous solution (5 mM, 10 mL) and ligand (5 mM, 10 mL) chloroform solution. The substrates were washed with water and dried with nitrogen stream after each immersion.

### 2.3 Analysis of Pd in (Pd/Ligand)<sub>n</sub> metal-organic films

The quartz slide coated with (Pd/Ligand)<sub>n</sub> was dissolved by aqua regia (10 ml). The Pd content was determined by inductively coupled plasma OES spectrometer (ICP-OES).

### 2.4 Typical procedure for the hydrogenation of olefin

Hydrogenation reactions were carried out in a hydrogen atmosphere (1.2 atm) at 34 °C. Typically, olefin (0.5 mmol), absolute ethanol (10 ml) and the quartz slide coated with (Pd/Ligand)<sub>10</sub> film were added to the tube. The tube was sealed with a teflon cap and evacuated and backfilled with H<sub>2</sub> three times. The mixture was stirred at a constant stirring speed (500 r/min) in the tube under an H<sub>2</sub> atmosphere. The conversion and yield were determined by GC analysis (430 GC). The ethanol solvent was removed under reduced pressure. The product was confirmed by <sup>1</sup>H spectroscopy.

### 2.5 Instrument

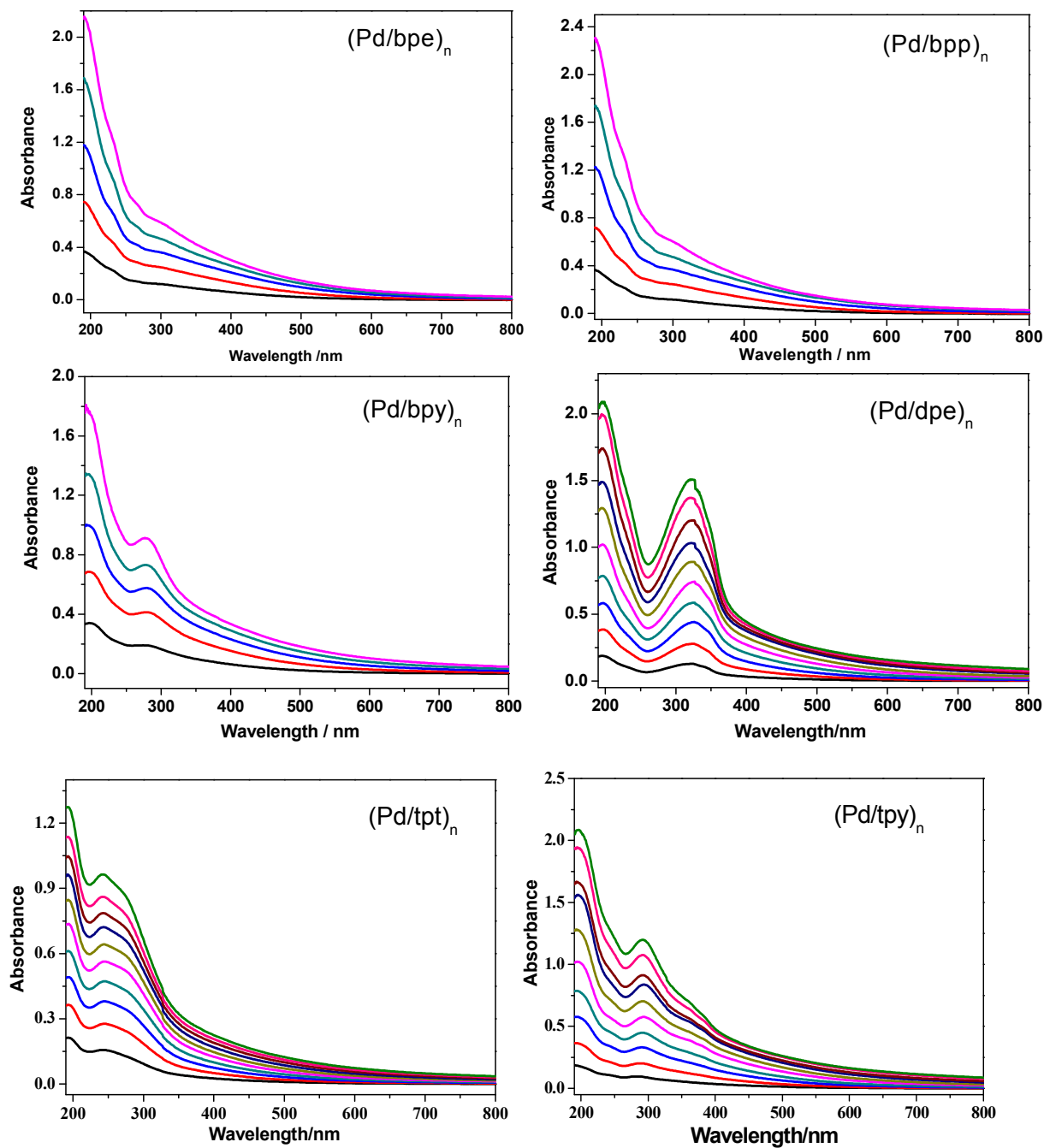
UV-vis absorption spectra were recorded on a quartz slide with a Lambda35 spectrophotometer (Perkin-Elmer, USA). All AFM images were taken on a single-crystal silicon slide using a Veeco Multimode NS3A-02NanoscopeIII atomic force microscope with silicon tips. Height images of the films were recorded using tapping-mode AFM. High-resolution X-ray photoelectron spectra (XPS) were collected at a takeoff angle of  $45^\circ$  using PHI Quantum 2000 scanning ESCA microprobe (Physical Electronics, USA) with an  $Al\alpha$  X-ray line (1486.6 eV). Transmission electron microscopy (TEM) was generated on a JEM-2010 operated at 120 kV. Small pieces of a multilayer film were scraped off the quartz substrate in ethanol and transferred to a copper grid. Gas chromatography-mass spectrometry (GC-MS) was performed on 430 GC (Varian, USA).  $^1H$  NMR (400 MHz) spectra were obtained on a Bruker AVANCE 400 spectrometer. Analysis of noble metal content was measured by inductively coupled plasma OES spectrometer (ICP-OES) (Ultima2, France).

### 3 Results and discussion

#### 3.1 Preparation and characterization

The multilayer films of (metal ions/Ligand)<sub>n</sub> were prepared by alternately immersing quartz slide pre-coated with PEI layer in metal ions aqueous solution and pyridyl ligand solution. Metal ion precursor is  $K_2PdCl_4$ . The self-assembly of (metal ions/Ligand)<sub>n</sub> films is based on the coordination bond between metal ions and the terminal pyridyl groups of ligand. The Pd ions were connected with ligand molecules. Metal–organic coordination interactions are responsible for the LbL deposition between palladium ions and the ligand molecules. The films (Pd/Ligand)<sub>n</sub> were characterized by UV-vis spectra. As shown in figure 1, different structures of ligands result in various peaks of UV-vis spectra. The absorbance of films is ascribed to the transition of  $\pi$  to

$\pi$  or  $n$  to  $\pi$  of ligand molecules. For non-conjugate ligands of bpp and bpe, the characteristics peaks of UV-vis spectra are not obvious. However, for conjugate groups of ligands (i.e., bpy, dpe, tpt, tpy and bitpy), the characteristics peaks were obviously observed and varied from the difference of structures. The peaks were labelled in figure S1 (See ESI). Furthermore, the UV absorbance of (Pd/Ligand)<sub>n</sub> films increases linearly with the number of bilayers of metal ions/Ligand, respectively (See figure S1 in ESI). The film growth shows a good linear correlation with  $R^2 = 0.99$  between the optical absorption and the number of ligand layers suggesting the ligand is incorporated into the films with a regular growth ( $R^2$  is a statistical calculation used with linear regressions). From UV-vis spectra, the deposition mechanism of (Pd/Ligand)<sub>n</sub> multilayers is perfect layer-by-layer self-assembling with complete surface coverage by plotting absorbance vs. number of Pd/Ligand bilayers,<sup>24</sup> which was further demonstrated by the AFMs below. In other words, all ligand molecules coordinate with Pd when depositing the ligand layer. In order to confirm the uniform LbL process, ICP-OES of Pd in 2, 4, 6, 8 and 10 bilayers were measured (See ESI, Table S1). Pd content increases linearly with an increasing number of bilayers and Pd content of each bilayer increases equably. This further demonstrates that the films are uniform LbL process.



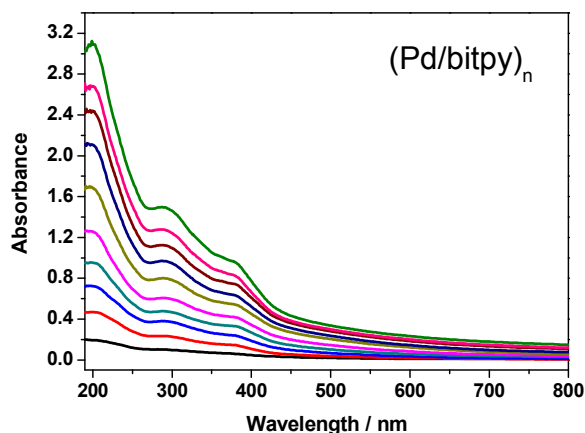


**Fig. 1** UV-vis spectra of  $(\text{Pd/Ligand})_n$ .

The surface morphology information was characterized by the atomic force microscopy (AFM) images (Figure 2). The AFM images provide valuable information about surface topographic images at the molecular level. As seen in AFMs, clearly, the silicon surface with  $(\text{Pd/Ligand})_5$  appears to be very smooth and large aggregate particles are not obviously observed. The distribution of the particles is uniform and compact. Moreover, the root-mean-square (RMS) roughness changed little for different structure of ligands. For example, the RMS roughness of  $(\text{Pd/bpe})_5$  and  $(\text{Pd/dpe})_5$  films is 6.20 nm and 6.36 nm, respectively. The  $(\text{Pd/bitpy})_5$  films with rigid conjugated ligand bitpy shows larger RMS of 8.62 nm. In general, the RMS roughness of films changed very little from 6.20 nm to 8.62 nm. The above-mentioned results further demonstrated that the deposition mechanism of these films is perfect layer-by-layer self-assembling with complete surface coverage. Only complete surface coverage results in the uniform surface without surface defects, consistent with the results of UV-vis spectra.

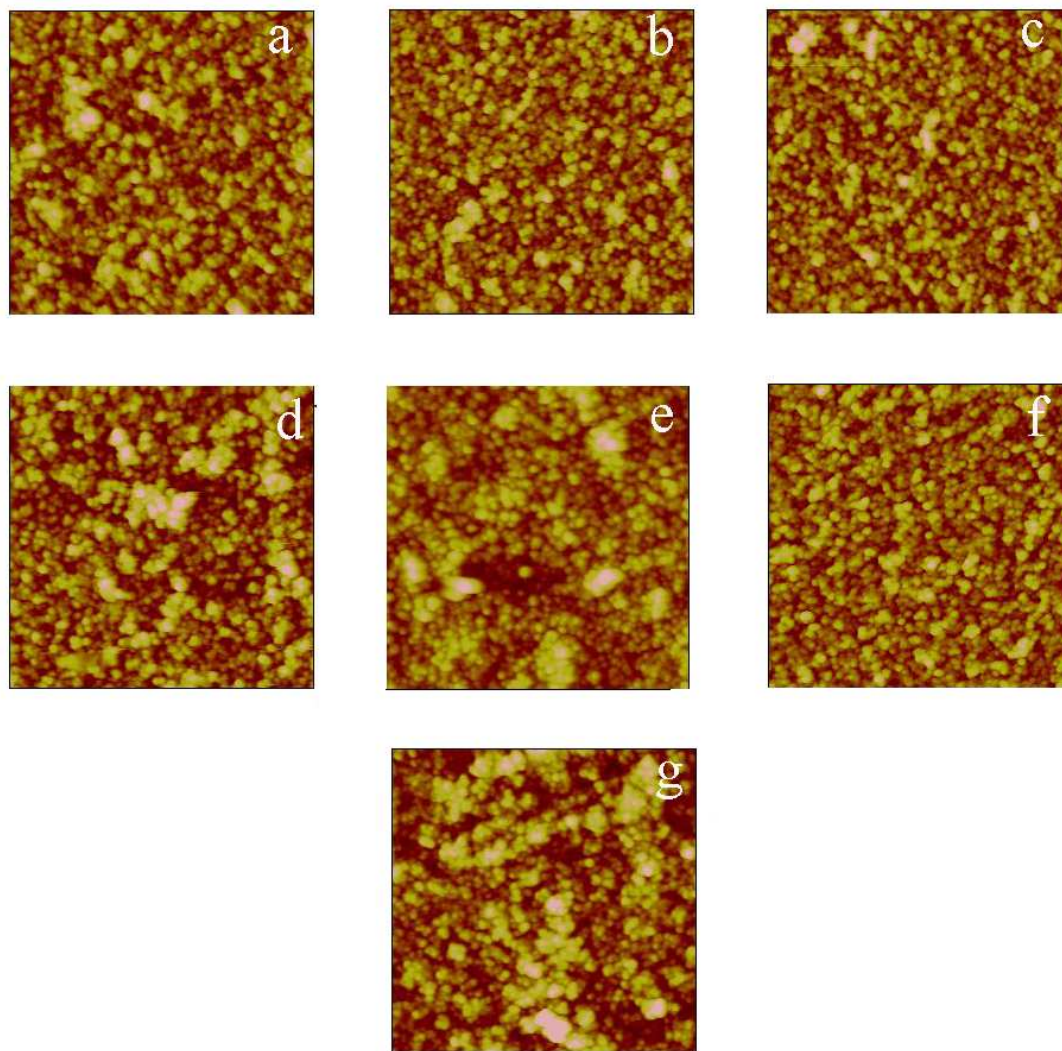


**Fig. 2** Typical height images of the films on the single-crystal silicon substrate (scan area is  $1.0 \times 1.0 \mu\text{m}^2$ , Z range: 50 nm). (a) (Pd/bpy)<sub>5</sub> ( $R_{\text{rms}} = 8.04$  nm), (b) (Pd/bpe)<sub>5</sub> ( $R_{\text{rms}} = 6.20$  nm), (c) (Pd/dpe)<sub>5</sub> ( $R_{\text{rms}} = 6.36$  nm), (d) (Pd/bpp)<sub>5</sub> ( $R_{\text{rms}} = 7.84$  nm), (e) (Pd/tpt)<sub>5</sub> ( $R_{\text{rms}} = 6.33$  nm), (f) (Pd/tpy)<sub>5</sub> ( $R_{\text{rms}} = 7.61$  nm), (g) (Pd/bitpy)<sub>5</sub> ( $R_{\text{rms}} = 8.62$  nm).

### 3.2 Catalytic performance of films for the hydrogenation of styrene

Hydrogenation of alkenes is important due to its industrial applications such as petroleum processing.<sup>25, 26</sup> Using our as-prepared film catalysts, the olefin hydrogenation was explored. Styrene hydrogenation was applied as a test reaction to study the catalytic activity of the films.

Pd content was detected through ICP-OES. Pd content and TON of different ligands are shown in Table 1. Pd content of both (Pd/bpy)<sub>10</sub> and (Pd/bpe)<sub>10</sub> multilayers is  $4.2 \times 10^{-7}$  mol. For monodentate pyridyl ligands dpe and bpp, it was found that Pd content is similar. The maximum content of Pd is  $5.8 \times 10^{-7}$  mol for tridentate ligand of bitpy. For (Pd/tpt)<sub>10</sub>, Pd content is minimum due to larger steric hindrance of tpt. Turnover number (TON) (moles of substrate converted per mole of catalyst) can be calculated by

$$\text{TON} = \frac{\text{Number of molecules reacted}}{\text{Number of catalyst}}$$

The TON represents the maximum yield of products attainable from a catalytic center.<sup>27</sup> Therefore, TON of (Pd/bpy)<sub>10</sub> films is calculated for 1190. The maximum TON value is from (Pd/bpp)<sub>10</sub> films due to small steric hindrance of monodentate pyridyl and the increase of alkyl moieties. In contrast, the minimum TON value is from (Pd/bitpy)<sub>10</sub> films due to tridentate ligand of bitpy. Under the same reaction conditions, TON of the 5% Pd/C reference catalyst ( $9.8 \times 10^{-7}$  mol) is 510. Compared with traditional heterogeneous catalysts in the reported references,<sup>28, 29</sup> such as Pd NPs/PEG with 660 TON and Pd NPs/MOF-5 with 682 TON, our metal-organic films not only have higher TON values, but also are easily removed from the reaction mixture without separation filtration. The reusability of (Pd/bpy)<sub>10</sub> films was investigated. After completion of a catalytic reaction, solid glass slides modified with (Pd/bpy)<sub>10</sub> films were simply removed from the product, washed with ethanol, dried, and then reused in another catalytic cycle using fresh styrene/ethanol mixture. This process was repeated for at least 10 cycles for the hydrogenation of styrene (See ESI, Figure S2). The results show that our film catalysts have good recyclability and the recycling is more convenient as compared to the traditional heterogeneous catalysts.

In order to demonstrate if the reaction proceeded in a heterogeneous or homogeneous fashion, the measurement of the Pd leaching was performed. The (Pd/bpy)<sub>10</sub> catalysts were removed during the reaction course (15 min for the styrene hydrogenation reaction, 2 h for the nitrobenzene hydrogenation reaction) and the reaction mixtures were kept to react under identical reaction conditions (30 min for the styrene hydrogenation and 4 h for the nitrobenzene hydrogenation). The substrate conversion remained unchanged after the removal of catalysts from the reaction systems. It demonstrates that no soluble species leaching from film act as the true catalysts, which indicates that the film catalysts proceeded in a heterogeneous fashion. In addition, inductively coupled plasma-mass spectrometry (ICP-MS) of supernatant for the reaction mixtures (10 mL) was performed. After 5.5 h, nitrobenzene was completely hydrogenated into aniline by (Pd/bpy)<sub>10</sub> film catalysts and the aniline/ethanol supernatant was used to analyze the ICP-MS. The results show that the concentration of Pd in the reaction mixtures is very low (0.081 ppm). This demonstrates that the amount of Pd leaching into the reaction system is negligible and the films have good stability.

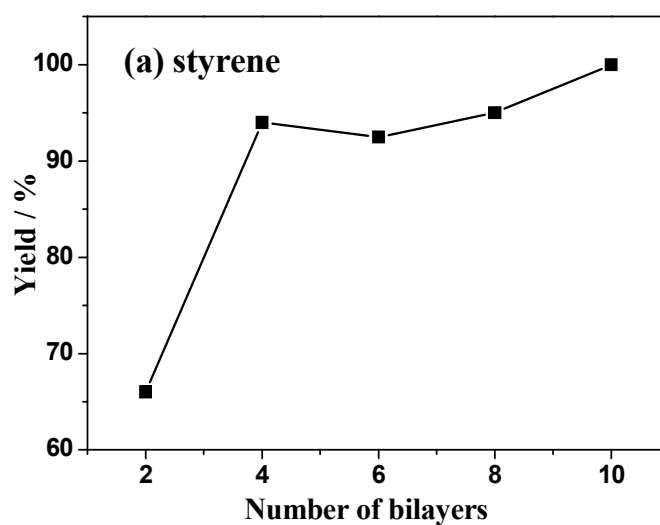
**Table 1** Pd content and TON of different films

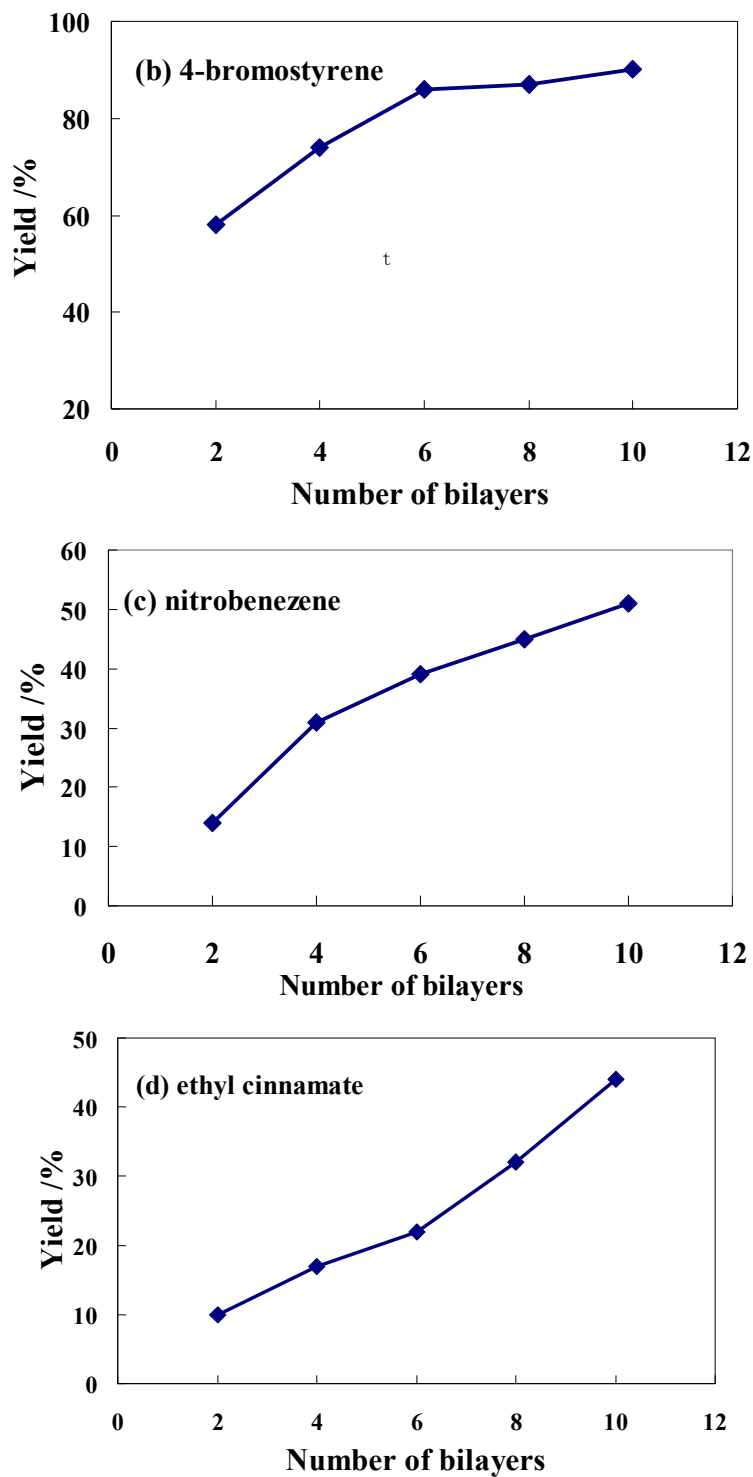
	(Pd/bpy) <sub>10</sub>	(Pd/bpe) <sub>10</sub>	(Pd/dpe) <sub>10</sub>	(Pd/bpp) <sub>10</sub>	(Pd/tpt) <sub>10</sub>	(Pd/tpy) <sub>10</sub>	(Pd/bitpy) <sub>10</sub>
Pd (mol)	$4.2 \times 10^{-7}$	$4.2 \times 10^{-7}$	$4.4 \times 10^{-7}$	$4.1 \times 10^{-7}$	$3.8 \times 10^{-7}$	$5.3 \times 10^{-7}$	$5.8 \times 10^{-7}$
TON	1190	1190	1136	1219	1316	943	862

Turnover number (TON) : moles of substrate converted per mole of catalyst.

Several substrate molecules were used as the test substrates to investigate the relationship between the substrate conversion and the number of (Pd/bpy)<sub>n</sub> bilayers (Figure 3). For styrene, the results show that the hydrogenation of styrene proceeds smoothly and completely to give ethylbenzene without any detectable byproducts during the time of 30 min. The catalytic activity

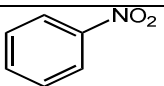
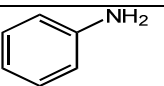
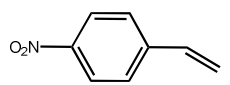
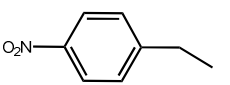
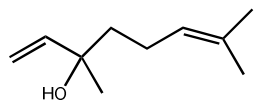
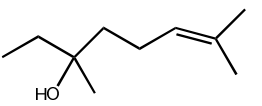
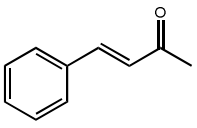
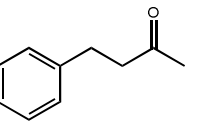
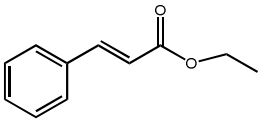
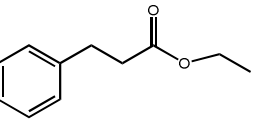
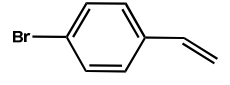
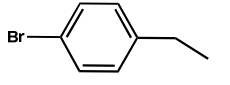
of the films increases with the number of bilayers. However, after the number of  $(\text{Pd/bpy})_n$  bilayers is 4, the conversion of styrene hydrogenation increases slowly (Figure 3a), whereas the conversion of 4-bromostyrene hydrogenation remains unchanged after the number of  $(\text{Pd/bpy})_n$  bilayers is 6 (Figure 3b). In contrast, the conversion increases with the number of bilayers for nitrobenzene and ethyl cinnamate (Figure 3c and d). Therefore, the catalytic activity of the films correlates with the number of bilayers. In other words, the catalytic activity is related to the loading amount of catalysts. The films of more bilayers have higher efficiency. Besides, there is a more important factor influencing the catalytic activity for styrene and 4-bromostyrene. The hydrogenation conversion remains unchanged after the multilayers reach a certain bilayer. This indicates that the catalytic activity is also related to the permeability of the substrate molecule into the film. Some substrate molecules are permeable through a certain number of bilayers and difficult to penetrate into the inner multilayers due to the increasing of penetration resistance. When the multilayers reach more bilayer, the substrate molecule can not enter into the inner multilayers. Therefore, both the loading amount of catalysts and the permeability simultaneously influence the catalytic activity.





**Fig. 3** Relationship between different substrate conversion and the number of  $(\text{Pd}/\text{bpy})_n$  bilayers for a certain time. (a) 30 min, (b) 110 min, (c) 120 min, (d) 120 min.

**Table 2** Hydrogenation of olefin and nitrobenzene over film catalysts (Pd/bpy)<sub>10</sub>

entry	Substrate	Product	Time	Yield (%) <sup>a</sup>
1			5.3 h	>99
2			7.5 h	85
3			3 h	95
4			8.5 h	91
5			5 h	>99
6			2.5 h	99
7			8.0 h	92

Reaction conditions: substrate (0.5 mmol), absolute ethanol (10 ml), stirring, H<sub>2</sub> (1.2 atm), 34°C.

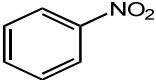
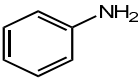
<sup>a</sup> Determined by GC methods.

### 3.3 Effect of the substrates

Besides styrene, the hydrogenation of other olefin substrates was investigated using our film catalysts in order to explore the scope of the catalytic reactions. The results are summarized in Table 1. The selectivity is not listed, because the selectivity of the product reaches more than 99%. For example, 3, 7-dimethyl-1,6-octadien-3-ol is selectively hydrogenated to 3,7-dimethyl-6-octen-3-ol (Table 2, entry 3), in which the allyl alcohol are difficultly hydrogenated due to steric hindrance of  $\alpha$  position to the double bond. Benzalacetone and ethyl cinnamate is selectively hydrogenated (Table 2, entries 4-5). Nitrobenzene is reduced into

aniline (Table 2, entry 1). Especially for cyclohexene hydrogenation, our pyridyl film (Pd/bpy)<sub>10</sub> exhibits the catalytic efficiency (Table 2, entry 7).

**Table 3** Hydrogenation of olefin and nitrobenzene over different film catalysts

entry	Substrate	Product	Catalyst	Time	Yield (%) <sup>a</sup>	TOF (h <sup>-1</sup> )
1			(Pd/bpy) <sub>10</sub>	5.3 h	>99	224
			(Pd/bpe) <sub>10</sub>	5.0 h	>99	238
			(Pd/dpe) <sub>10</sub>	5.0 h	>99	227
			(Pd/bpp) <sub>10</sub>	5.0 h	>99	244
			(Pd/tpt) <sub>10</sub>	5.75 h	>99	228
			(Pd/tpy) <sub>10</sub>	9.0 h	>99	104
			(Pd/bitpy) <sub>10</sub>	7.5 h	>99	114
			(Pd/bpy) <sub>10</sub>	8.0 h	92	137
2			(Pd/dpe) <sub>10</sub>	6.5 h	91	159
			(Pd/bpp) <sub>10</sub>	6.0 h	92	187
			(Pd/tpt) <sub>10</sub>	9.0 h	86	125
			(Pd/tpy) <sub>10</sub>	13.0 h	62	45
			(Pd/bpy) <sub>10</sub>	7.0 h	93	158
			(Pd/bitpy) <sub>10</sub>	7.6 h	86	97

Reaction conditions: substrate (0.5 mmol), absolute ethanol (10 ml), stirring, H<sub>2</sub> (1.2 atm), 34°C. <sup>a</sup> Determined by GC methods. TOF: moles of substrate converted per mole of catalyst per h.

The influence of different ligand structures on the catalytic properties was also explored. The results are listed in Table 3. For monodentate ligands such as bpy, bpe and bpp, the catalytic activity is similar. With the increase of alkyl moieties (i.e., from bpy to bpp), the catalytic activity is increasing. In case of tridentate ligands such as tpy and bitpy, the catalytic activity is lower than monodentate ligands. This is because three pyridyl groups of tpy and bitpy all coordinate to Pd ions. For nitrobenzene and cyclohexene hydrogenation, the films (Pd/bpp)<sub>10</sub>

have the highest TOF, indicating that the films constructed by bpp molecules exhibited better catalytic activity. The films of tpy molecules have the lowest TOF. This is related to the coordination mode of ligand. One pyridyl group of the monodentate ligand is coordinated to the Pd ion. In other words, the Pd ion is coordinated to two different pyridyl groups. In general, Pd ions are four-connected. Thus, there was two non coordinate free vacancy. When the catalytic substrate molecule attack Pd ions, two non coordinate free vacancy of Pd ions are easily occupied by the substrate molecules. With the increasement of the alkyl group of monodentate ligands, the attack steric hindrance becomes smaller. Thus, it exhibits better catalytic activity. In contrast, for tridentate ligands, the Pd ion is all coordinated to pyridyl groups and have no coordinate free vacancy. When the catalytic substrate molecule attack Pd ions, it competes against coordinated pyridyl groups. This largely increases the resistance and results in lower catalytic activity.

Our metal complex films were explored as a highly active and recyclable catalyst for hydrogenation of olefin under mild conditions. The reasons as a highly efficient catalyst were investigated by TEM and XPS in detail. During the process of olefin hydrogenation, hydrogen gas was used as a reductant for metal ions besides hydrogen source for the hydrogenation reactions. The specific reduction process was clearly explained by (Pd/bpy)<sub>n</sub> films. The reduction process of Pd(II) to Pd(0) in the LbL multilayers was further characterized by XPS and TEM. Significant difference was recorded for the Pd/bpy multilayers before and after reduction from XPS. The peak position and intensity for the elements of Pd largely changes before and after the hydrogen reduction. Before the styrene hydrogenation reaction, the peaks with the binding energy 337.0/342.4 eV (Figure 4a) ascribing to Pd(II) are observed. After the 10th cycle of styrene hydrogenation, a couple of new peaks at 335.3/340.5 eV with high intensity are ascribed to Pd(0) (Figure 4b), indicating that Pd(II) ions are reduced to Pd(0).<sup>30</sup> A couple of peaks at

337.0/342.4 eV with very low intensity are ascribed to Pd(II). With the increase of cycle numbers, it is predicted that the peaks at 337.0/342.4 eV completely disappear and those at 335.3/340.5 eV largely increase, indicating that all Pd(II) ions are reduced into Pd(0) (Figure 4b).

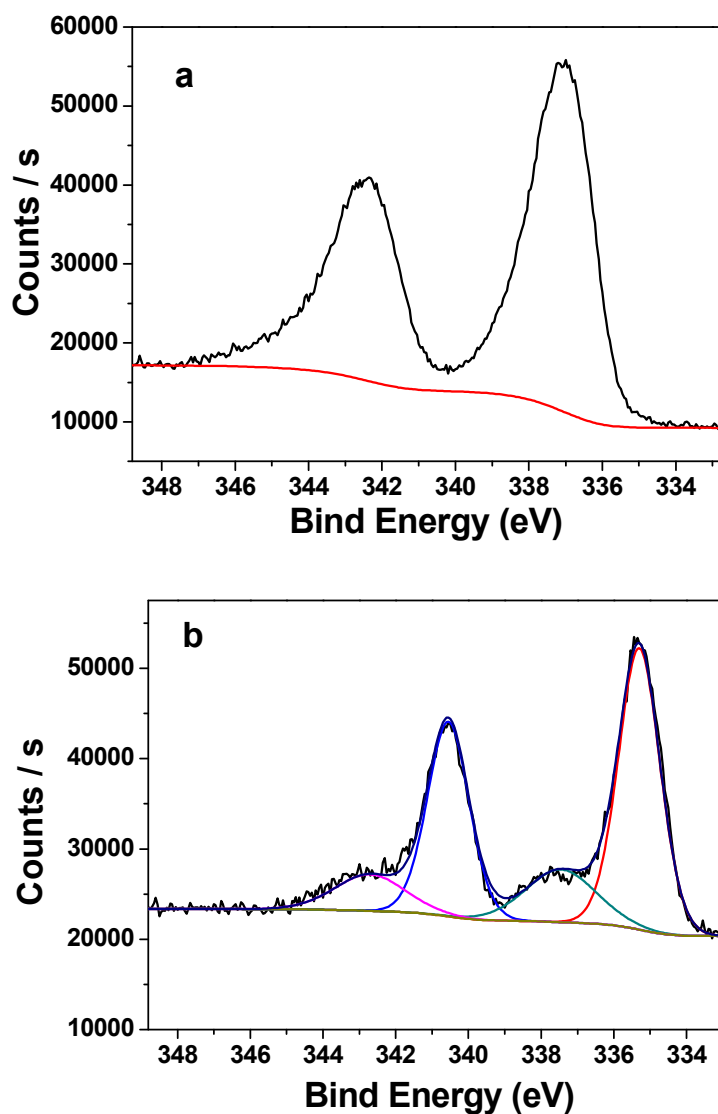


**Fig. 4** XPS spectra of the Pd<sub>3d</sub> region for (Pd/bpy)<sub>10</sub> film deposited on the solid glass substrate before styrene hydrogenation (a) and after the 10<sup>th</sup> cycle of styrene hydrogenation (b).

Based on the above analysis, metal ions are gradually reduced into NPs. As shown in TEM images, for (Pd/Ligand)<sub>10</sub> films, NPs tend to aggregate after the hydrogenation (Figure 5). The analysis of TEM results further demonstrates that Pd(II) ions are gradually converted to Pd(0) states during the process of hydrogenation. During the hydrogenation process, metal ions are firstly *in situ* reduced into atoms encapsulated in multilayers in hydrogen gas aqueous solution.<sup>31</sup> The single atoms separated from bpy molecules have high energy and high catalytic activity.<sup>32</sup> The atoms tend to reduce its energy. In other words, metal atoms with high energy tend to form small NPs with slightly low energy and lower activity under the external conditions. On the other hand, NPs are more easily dispersed by the pyridyl ligand to avoid aggregation. Thus, it results in high activity of films.

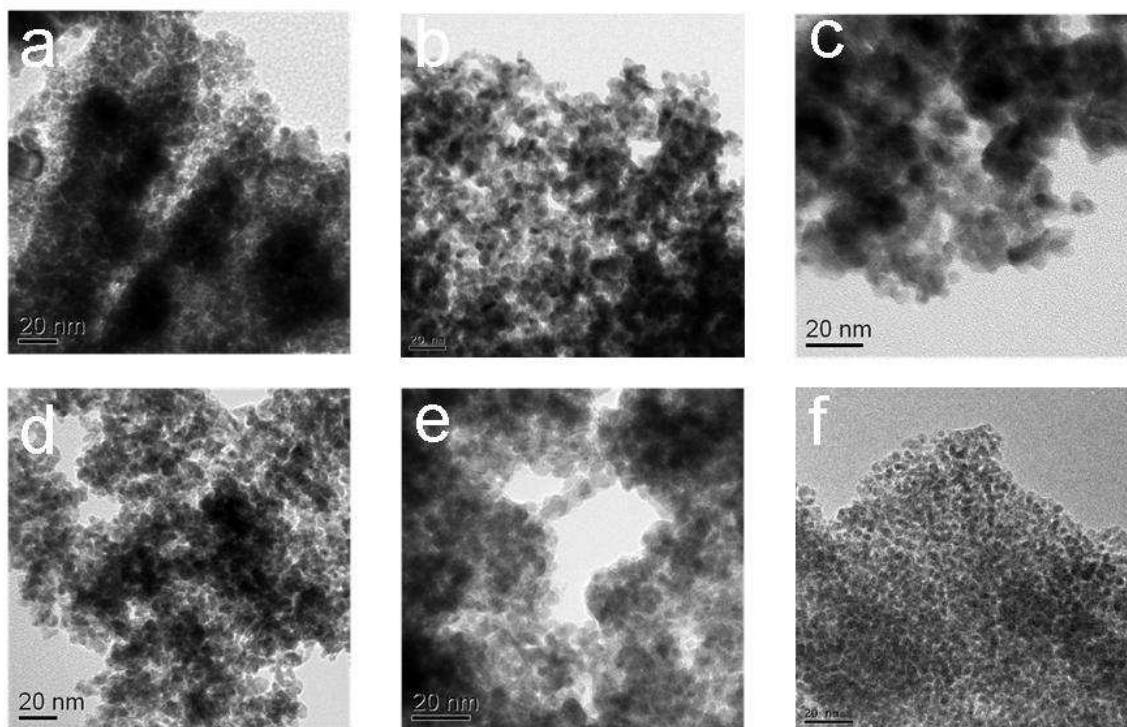


**Fig. 5** TEM images of films after nitrobenzene hydrogenation. (a) (Pd/bpy)<sub>10</sub>, (b) (Pd/bpe)<sub>10</sub>, (c) (Pd/bpp)<sub>10</sub>, (d) (Pd/tpt)<sub>10</sub>, (e) (Pd/tpy)<sub>10</sub>, (f) (Pd/bitpy)<sub>10</sub>.

As shown in TEM images, for monodentate ligands (i.e., bpy, bpe and bpp) (Figure 5a-c), NPs tend to aggregate after the hydrogenation and become larger, whereas NPs are not easy to aggregate and the size of NPs is smaller for tridentate ligands (Figure 5e-f). It is related to the coordination mode of films. For monodentate ligands, Pd ions are coordinated to two pyridyl groups, whereas Pd ions are coordinated to four or six pyridyl groups of tridentate ligands. Thus, Pd ions of tridentate ligands are more firmly bonded than that of monodentate ligands. The dispersion of particles in (Pd/bitpy)<sub>10</sub> films is more uniform. As seen in AFMs (Figure 6), the obvious aggregates occur after the hydrogenation, consistent with TEM images.

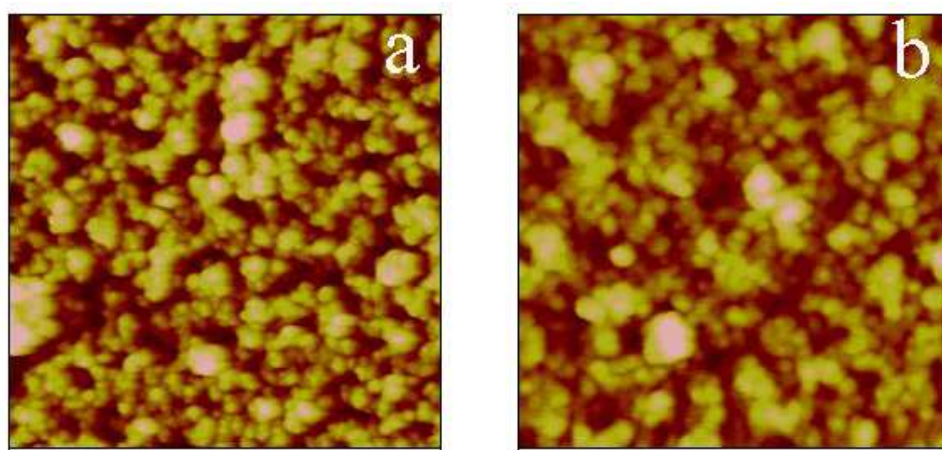


**Fig. 6** Typical height images of the films on a solid glass substrate after hydrogenation. (a) (Pd/bpe)<sub>10</sub>, (b) (Pd/bitpy)<sub>10</sub>

#### 4 Conclusions

In the present work, palladium NPs *in situ* generated in metal-organic films were described for catalytic applications. Metal-organic films were characterized by UV-vis spectra and atomic force images (AFMs). Metal-organic films containing Pd ions shows a uniform and regular

growth. TEM results also further demonstrated that Pd NPs were *in situ* formed in metal-organic films during catalytic hydrogenation process. The resulting films displayed the catalytic properties. The results show that the catalytic films exhibit a superior catalytic activity toward hydrogenation of various type of olefin under mild conditions. In view of activity, the monodentate bipyridyl ligands films exhibit better performance than that of tridentate polypyridyl films. The catalytic activity of films is related to the number of bilayers and permeability. Moreover, our catalytic films have the superiority compared with traditional heterogeneous catalysts, due to ease of catalyst separation and good recyclability.

## Acknowledgements

This work was financially supported by 973 Program (2011CB932504 and 2012CB821705), NSFC (21173222, 21221001 and 21203199), Fujian Key laboratory of Nanomaterials (2006L2005), the Key Project from CAS.

Electronic Supplementary Information (ESI) available:  $^1\text{H}$  NMR and GC-MS spectra of the product. See DOI: 10.1039/b000000x/

## Notes and references

- 1 X. Wang, G. Wu, N. Guan and L. Li, *Appl. Catal. B*, 2012, **115**, 7-15.
- 2 F. A. Harraz, S. E. El-Hout, H. M. Killa and I. A. Ibrahim, *J. Catal.*, 2012, **286**, 184-192.
- 3 M. Lim, K. A. De Castro, S. Oh, K. Lee, Y.-W. Chang, H. Kim and H. Rhee, *Appl. Organometal. Chem.*, 2011, **25**, 1-8.
- 4 F. Menegazzo, M. Signoretto, G. Frison, F. Pinna, G. Strukul, M. Manzoli and F. Boccuzzi, *J. Catal.*, 2012, **290**, 143-150.

- 5 T. Shamim, M. Gupta and S. Paul, *J. Mol. Catal. A: Chem.*, 2009, **302**, 15-19.
- 6 C. A. McNamara, M. J. Dixon and M. Bradley, *Chem. Rev.*, 2002, **102**, 3275-3300.
- 7 M. Benaglia, A. Puglisi and F. Cozzi, *Chem. Rev.*, 2003, **103**, 3401-3430.
- 8 A. Mentbayeva, A. Ospanova, Z. Tashmuhambetova, V. Sokolova and S. Sukhishvili, *Langmuir*, 2012, **28**, 11948-11955.
- 9 H. Krass, E. A. Plummer, J. M. Haider, P. R. Barker, N. W. Alcock, Z. Pikamenou, M. J. Hannon and D. G. Kurth, *Angew. Chem. Int. Ed.*, 2001, **40**, 3862-3865.
- 10 H. Krass, G. Papastavrou and D. G. Kurth, *Chem. Mater.*, 2003, **15**, 196-203.
- 11 G. Decher, *Science*, 1997, **277**, 1232-1237.
- 12 M. Altman, A. D. Shukla, T. Zubkov, G. Evmenenko, P. Dutta and M. E. van der Boom, *J. Am. Chem. Soc.*, 2006, **128**, 7374-7382.
- 13 J. Choudhury, R. Kaminker, L. Motiei, G. de Ruyter, M. Morozov, F. Lupo, A. Guilino and M. E. van der Boom, *J. Am. Chem. Soc.*, 2010, **132**, 9295-9297.
- 14 S. Gao, Z. Zheng, J. Lü and R. Cao, *Chem. Commun.*, 2010, **46**, 7584-7586.
- 15 J. Pan, B. Tong, J. Shi, W. Zhao, J. Shen, J. Zhi and Y. Dong, *J. Phys. Chem. C*, 2010, **114**, 8040-8047.
- 16 W. Zhao, B. Tong, Y. Pan, J. Shen, J. Zhi and Y. Dong, *Langmuir*, 2009, **25**, 11796-11801.
- 17 A. Maier and T. Bernd, *J. Phys. Chem. B.*, 2012, **116**, 925-934.
- 18 S. Kidambi, J. Dai, J. Li and M. L. Bruening, *J. Am. Chem. Soc.*, 2004, **126**, 2658-2659.
- 19 S. Kidambi and M. L. Bruening, *Chem. Mater.*, 2005, **17**, 301-307.
- 20 S. Bhattacharjee and M. L. Bruening, *Langmuir*, **2008**, **24**, 2916-2920.
- 21 Y. Wang and J-K. Lee, *J. Mol. Catal. A: Chem.*, **2007**, **263**, 163-168.

- 22 Z. Ren, H.-L. Wang, Y.-Q. Cai, M. Chen and D.-J. Qian, *Mater. Chem. Phys.*, 2011, **127**, 310-315.
- 23 J. H. Wang and G. S. Hanan, *Synlett*, 2005, **8**, 1251-1254.
- 24 J.-F. Koenig and D. Martel, *Thin Solid Films*, 2008, **516**, 3865-3877.
- 25 D. Li, *Chinese J. Catal.*, 2013, **34**, 48-60.
- 26 F. Pinto, S. Martins, M. Gonçalves, P. Costa, I. Gulyurtlu, A. Alves and B. Mendes, *Appl. Energ.*, 2013, **102**, 272-282.
- 27 S. Kozuch and J. M. L. Martin, *ACS Catal.*, 2012, **2**, 2787-2794.
- 28 F. A. Harraz, S. E. El-Hout, H. M. Killa and I. A. Ibrahim, *J. Catal.*, 2012, **286**, 184-192.
- 29 Y. Pan, D. Ma, H. Liu, H. Wu, D. He and Y. Li, *J. Mater. Chem.*, 2012, **22**, 10834-10839.
- 30 S. Kidambi and M. L. Bruening, *Chem. Mater.*, 2005, **17**, 301-307.
- 31 C. W. Scheeren, G. Machado, S. R. Teixeira, J. Morais, J. B. Domingos and J. Dupont, *J. Phys. Chem. B*, 2006, **110**, 13011-13020.
- 32 D.-J. Qian, T. Wakayama, C. Nakamura and J. Miyake, *J. Phys. Chem. B.*, 2003, **107**, 3333-3335.

Entry for the Table of Contents

## Palladium nanoparticles *in situ* generated in metal-organic films for catalytic applications

Shuiying Gao, Minna Cao, Weijin Li and Rong Cao

Palladium nanoparticles were firstly *in situ* generated in metal-organic films for catalytic applications.

